Journal of Thermal Analysis and Calorimetry (2020) 139:741–754
https://doi.org/10.1007/s10973-019-08404-4

Effect of a porous medium on flow and mixed convection heat transfer of nanofluids with variable properties in a trapezoidal enclosure

Abdullah A. A. A. Al-Rashed[1] · Ghanbar Ali Sheikhzadeh[2] · Alireza Aghaei[3] · Farhad Monfared[2] · Amin Shahsavar[4] · Masoud Afrand[5,6]

Received: 9 February 2019 / Accepted: 22 May 2019 / Published online: 3 June 2019

Abstract

In the present study, the flow field and heat transfer of a water–copper nanofluid with variable properties in a trapezoidal enclosure saturated with porous media are studied. The governing equations are solved by finite volume method and the SIMPLER algorithm. The nanofluid flow is assumed to be laminar, steady and incompressible. Simulations are performed for sidewall (trapezoid legs) angles of 30°, 45° and 60° with respect to horizontal axis, Reynolds numbers from 10 to 1000, Darcy numbers of 10^{-2}, 10^{-3}, 10^{-4} and volume fractions of 0 to 0.04 of nanoparticles. Numerical results show that the average Nusselt number increases with increasing volume fraction of nanoparticles for all studied Darcy numbers. The convection and motion of the nanofluid decrease by reducing the Darcy number which leads to a reduction in the velocity and local Nusselt number. The average Nusselt number increases by increasing the Darcy number for all aspect ratios. Also, the average Nusselt number increases with increasing Reynolds number for all Darcy numbers, aspect ratios and volume fractions of nanoparticles.

Keywords Porous medium · Nanofluid · Trapezius enclosure · Numerical solution · Mixed convection · Darcy number

Introduction

The fluid flow and heat transfer in an enclosure filled with porous media have widely attracted interest of many researchers. Insulation materials, geophysical applications, heating and cooling in buildings, underground heat pump systems and solar energy are examples of fluid flows in porous mediums [1–4]. On the one hand, it has always been desirable to have access to smaller dimensions and higher returns for better heat transfer in industrial equipment such as electronic components and heat exchangers. On the other hand, it has always been desirable to have access to smaller dimensions and higher efficiency for higher heat transfer in industrial equipments such as electronic components and heat exchangers. In recent years, the study of material properties in a nanoscale has been more considered due to that the nanoparticles exhibit different behaviors from the macroscale. Dispersion of nanoparticles into common fluids such as water, oil and ethylene glycol may change the properties of colloid and improve heat transfer [5–21].

✉ Masoud Afrand
masoud.afrand@tdtu.edu.vn

1 Department of Automotive and Marine Engineering Technology, College of Technological Studies, The Public Authority for Applied Education and Training, Kuwait City, Kuwait

2 Department of Mechanical Engineering, University of Kashan, Kashan, Iran

3 Young Researchers and Elite Club, Arak Branch, Islamic Azad University, Arak, Iran

4 Department of Mechanical Engineering, Kermanshah University of Technology, Kermanshah, Iran

5 Laboratory of Magnetism and Magnetic Materials, Advanced Institute of Materials Science, Ton Duc Thang University, Ho Chi Minh City, Vietnam

6 Faculty of Applied Sciences, Ton Duc Thang University, Ho Chi Minh City, Vietnam

Mixed convection has many applications in nuclear reactors, industrial lubricants, heat exchangers, metal melting industries, etc., due to the combined effects of natural and forced convections. In particular, the cooling of elliptical heat resources is considered in the electronic industry and solar collectors [22].

Mansour et al. [23] studied mixed convection of a nanofluid in a cavity with a moving cold upper wall, cold sidewalls and a bottom wall in which constant heat flux was applied. According to their results, the fluid flow decreases by increasing the volume fraction of nanoparticles, but the average Nusselt increases.

Ghasemi and Aminossadati [24] studied the mixed convection of aluminum oxide–water in a triangular enclosure with horizontal insulated wall, vertical cold and moving wall in the up or down directions and hot inclined wall. According to their results, heat transfer increases by increasing the volume fraction of nanoparticles and moving the vertical wall in both directions for the whole studied range of the Richardson number.

Sheikhzadeh et al. [25] investigated the heat transfer and fluid flow of aluminum oxide–water nanofluid in a square box with moving upper wall, insulated horizontal walls and vertical walls with hot and cold temperatures on the right and left sides, respectively, numerically using finite volume method. Based on their results, by considering the variable properties of the thermal conductivity and fluid viscosity coefficients, the average Nusselt number changes compared to that for constant properties. In addition, they reported that the difference is larger for low Richardson numbers (0.01 and 0.1) than high Richardson numbers (10 and 100).

Pishkar and Ghasemi [26] studied mixed convection heat transfer and fluid flow in a horizontal channel with a blade for a water–copper nanofluid numerically. They found that the heat transfer increases by increasing the volume fraction and Reynolds number. This increase is higher at higher Reynolds numbers for a constant volume fraction.

Chamkha and Abu-Nada [27] investigated mixed convection heat transfer and fluid flow in a square enclosure with lateral insulated walls, hot upper and cold bottom walls for two cases. In the first case, only the upper horizontal wall was movable, and in the second case, the upper and lower horizontal walls moved in the opposite direction. They revealed that the average Nusselt number increases by increasing the volume fraction and decreasing the Richardson number.

Abbasian et al. [28] investigated mixed convection heat transfer and fluid flow of the water–copper nanofluid in a square enclosure in which the horizontal walls were insulated and the lateral walls had sinusoidal temperature boundary condition. Based on their results, the average Nusselt number increases with the increase in phase difference and the Richardson number for a constant volume fraction.

Oztop et al. [29] studied natural convection heat transfer and fluid flow in an opened cavity filled with porous media numerically. They demonstrated that the Nusselt number increases by increasing the Darcy number for all Rayleigh numbers.

Bourantas et al. [30] studied natural convection and heat transfer of a nanofluid with constant properties in square enclosures in porous media numerically. The bottom wall was under constant heat flux partially, and the other walls were cold. Based on their results, the average Nusselt number increases with increasing Rayleigh number for all Darcy numbers at a constant volume fraction.

Hajipour and Dehkordi [31] investigated mixed convection heat transfer of aluminum oxide–water in a channel filled with porous material experimentally and numerically. Their results differed from the previous studies.

Nielda and Kuznetsov [32] investigated the effect of Brownian motion and thermophoresis on forced convection of a nanofluid in a channel filled with porous media. Their results showed that Brownian motion and thermophoresis have opposite effects on the average Nusselt number.

In the present study, fluid flow and mixed convection heat transfer of a nanofluid with variable properties in a trapezoidal cavity filled with porous media are investigated numerically. The sidewalls of the enclosure are insulated, and the bottom and top walls are hot and cold, respectively. To analyze the mixed convection, a computer program written in FORTRAN, based on the finite volume method and SIMPLER algorithm, is used. This method has been used in the previous works [33–41] and was confirmed by the researchers. The Brinkman–Forchheimer model is used to model the porous media. The studies are conducted for various volume fractions of nanoparticles, Richardson and Darcy numbers and different aspect ratios.

Governing equations and boundary conditions

The schematic of the problem is shown in Fig. 1. The bottom wall of the enclosure is at the temperature T_h, the upper one is at the temperature T_c, and the sidewalls are insulated. The enclosure is filled with porous material. The nanofluid flow is assumed to be laminar, steady and incompressible. Simulations are performed for sidewall (trapezoid legs) angles of 30°, 45° and 60° with respect to

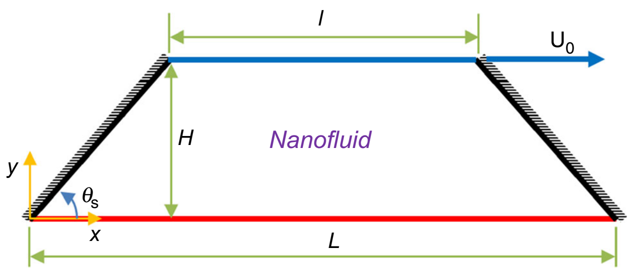

Fig. 1 Geometry of a two-dimensional trapezoidal cavity with insulated side walls, top moving wall and hot bottom wall filled with porous media

Table 1 Thermophysical properties of base fluid (at 300 K) and nanoparticles [42]

Property	Water (the base fluid)	Copper
c_p (J/kg K)	4179	385
ρ (kg/m^3)	997.1	8933
k (w/m K)	0.613	401
β (K^{-1})	21×10^{-5}	1.67×10^{-5}
μ (w/m K)	0.001003	–

horizontal axis, Reynolds numbers from 10 to 1000, Darcy numbers of 10^{-2}, 10^{-3}, 10^{-4} and volume fractions of 0–0.04.

Thermophysical properties of water as base fluid and copper nanoparticles are presented in Table 1.

The governing equations, including continuity, momentum and energy equations for Newtonian fluid and two-dimensional, laminar and steady flow, are defined as follows. The Brinkman–Forchheimer model is used to model the porous media.

$$\frac{\partial u}{\partial x}+\frac{\partial v}{\partial y}=0 \tag{1}$$

$$u\frac{\partial u}{\partial x}+v\frac{\partial u}{\partial y}=-\frac{1}{\rho_{\mathrm{nf}}}\frac{\partial p}{\partial x}+\frac{1}{\rho_{\mathrm{nf}}}\left[\frac{\partial}{\partial x}\left(\mu_{\mathrm{nf}}\frac{\partial u}{\partial x}\right)+\frac{\partial}{\partial y}\left(\mu_{\mathrm{nf}}\frac{\partial u}{\partial y}\right)\right]-\frac{\upsilon_{\mathrm{nf}}}{\varepsilon}u \tag{2}$$

$$u\frac{\partial v}{\partial x}+v\frac{\partial v}{\partial y}=-\frac{1}{\rho_{\mathrm{nf}}}\frac{\partial p}{\partial y}+\frac{1}{\rho_{\mathrm{nf}}}\left[\frac{\partial}{\partial x}\left(\mu_{\mathrm{nf}}\frac{\partial v}{\partial x}\right)+\frac{\partial}{\partial y}\left(\mu_{\mathrm{nf}}\frac{\partial v}{\partial y}\right)\right]+\frac{(\rho\beta)_{\mathrm{nf}}}{\rho_{\mathrm{nf}}}g(T-T_{\mathrm{c}})-\frac{\upsilon_{\mathrm{nf}}}{\varepsilon}v \tag{3}$$

$$u\frac{\partial T}{\partial x}+v\frac{\partial T}{\partial y}=-\frac{1}{(\rho c_{\mathrm{p}})_{\mathrm{nf}}}\left[\frac{\partial}{\partial x}\left(k_{\mathrm{nf}}\frac{\partial T}{\partial x}\right)+\frac{\partial}{\partial y}\left(k_{\mathrm{nf}}\frac{\partial T}{\partial y}\right)\right] \tag{4}$$

Since the problem is solved as a dimensionless manner, it is first necessary to non-dimensionlize the governing equations and boundary conditions. The quantities used for non-dimensionlizing are introduced in Eq. (5):

$$X=\frac{x}{H},\ Y=\frac{y}{H},\ V=\frac{v}{U_0},\ U=\frac{u}{U_0},\ \theta=\frac{T-T_{\mathrm{c}}}{T_{\mathrm{h}}-T_{\mathrm{c}}} \\ P=\frac{p}{\rho_{\mathrm{f}}U_0^2}, \tag{5}$$

$$\mathrm{Gr}=\frac{g\beta_{\mathrm{f}}H^3(T_{\mathrm{h}}-T_{\mathrm{c}})}{\upsilon_{\mathrm{f}}^2},\ Re=\frac{U_0H}{\upsilon_{\mathrm{f}}},\ \mathrm{Ri}=\frac{\mathrm{Gr}}{Re^2}=\frac{10^4}{Re^2},\ Pr=\frac{\upsilon_{\mathrm{f}}}{\alpha_{\mathrm{f}}},\ Da=\frac{\varepsilon}{H^2}$$

where ε represents the porosity of the medium and Da is dimensionless Darcy number. Reduction in the Darcy number indicates that the porosity of the media decreases. Using the dimensionless quantities, the equations for mass conservation, momentum and energy conservation are obtained:

$$\frac{\partial U}{\partial X}+\frac{\partial U}{\partial Y}=0 \tag{6}$$

$$U\frac{\partial U}{\partial X}+V\frac{\partial U}{\partial Y}=-\frac{\partial P}{\partial X}+\frac{1}{\rho_{\mathrm{nf}}\upsilon_{\mathrm{f}}Re}\left[\frac{\partial}{\partial X}\left(\mu_{\mathrm{nf}}\frac{\partial U}{\partial X}\right)+\frac{\partial}{\partial Y}\left(\mu_{\mathrm{nf}}\frac{\partial U}{\partial Y}\right)\right]-\frac{\upsilon_{\mathrm{nf}}}{\upsilon_{\mathrm{f}}}\frac{U}{Da\,H^2Re_{\mathrm{f}}} \tag{7}$$

$$U\frac{\partial V}{\partial X}+V\frac{\partial V}{\partial Y}=-\frac{\partial P}{\partial Y}+\frac{1}{\rho_{\mathrm{nf}}\upsilon_{\mathrm{f}}Re}\left[\frac{\partial}{\partial X}\left(\mu_{\mathrm{nf}}\frac{\partial V}{\partial X}\right)+\frac{\partial}{\partial Y}\left(\mu_{\mathrm{nf}}\frac{\partial V}{\partial Y}\right)\right]-\frac{\upsilon_{\mathrm{nf}}}{\upsilon_{\mathrm{f}}}\frac{V}{Da\,H^2Re_{\mathrm{f}}}+\frac{(\rho\beta)_{\mathrm{nf}}}{\rho_{\mathrm{nf}}\beta_{\mathrm{f}}}\mathrm{Ri}\theta \tag{8}$$

$$U\frac{\partial \theta}{\partial X}+V\frac{\partial \theta}{\partial Y}=\frac{1}{Re\,Pr\,\alpha_{\mathrm{f}}(\rho c_{\mathrm{p}})_{\mathrm{nf}}}\left[\frac{\partial}{\partial X}\left(k_{\mathrm{nf}}\frac{\partial \theta}{\partial X}\right)+\frac{\partial}{\partial Y}\left(k_{\mathrm{nf}}\frac{\partial \theta}{\partial Y}\right)\right] \tag{9}$$

According to the geometry of the problem, the boundary conditions are:

$$
\begin{array}{ll}
\text{On the bottom wall} & U = V = 0,\ \theta = 1 \\
\text{On the top wall} & U = 1,\ V = 0,\ \theta = 0 \\
\text{On the side walls } (n \text{ represents the normal direction}) & U = V = 0,\ \dfrac{\partial \theta}{\partial n} = 0
\end{array}
\tag{10}
$$

The nanofluid properties, including the density, thermal capacity, volumetric expansion coefficient, diffusion coefficient, the viscosity [43] and thermal conductivity coefficient [44], are obtained from relations (11)–(16), respectively.

$$\rho_{\mathrm{nf}} = (1-\varphi)\rho_{\mathrm{f}} + \varphi\rho_{\mathrm{s}} \tag{11}$$

$$\left(\rho c_{\mathrm{p}}\right)_{\mathrm{nf}} = (1-\varphi)\left(\rho c_{\mathrm{p}}\right)_{\mathrm{f}} + \varphi\left(\rho c_{\mathrm{p}}\right)_{\mathrm{s}} \tag{12}$$

$$(\rho\beta)_{\mathrm{nf}} = (1-\varphi)(\rho\beta)_{\mathrm{f}} + \varphi(\rho\beta)_{\mathrm{s}} \tag{13}$$

$$\alpha_{\mathrm{nf}} = \frac{k_{\mathrm{nf}}}{(\rho c_{\mathrm{P}})_{\mathrm{nf}}} \tag{14}$$

$$\mu_{\mathrm{nf}} = \mu_{\mathrm{f}}(1-\varphi)^{-2.5} \tag{15}$$

$$\frac{k_{\mathrm{eff}}}{k_{\mathrm{f}}} = 1 + \frac{k_{\mathrm{p}}A_{\mathrm{p}}}{k_{\mathrm{f}}A_{\mathrm{f}}} + Ck_{\mathrm{p}}Pe\frac{A_{\mathrm{p}}}{k_{\mathrm{f}}A_{\mathrm{f}}} \tag{16}$$

The effect of Brownian motion is appeared by considering the effect of temperature on thermal conductivity coefficient. The amount of thermal conductivity of the nanofluid by considering this effect is more than that when the effect of this motion is ignored. In (16), C = 36,000, $\frac{A_{\mathrm{p}}}{A_{\mathrm{f}}} = \frac{d_{\mathrm{f}}\varphi}{d_{\mathrm{p}}(1-\varphi)}$, $Pe = \frac{U_{\mathrm{p}}d_{\mathrm{p}}}{\alpha_{\mathrm{f}}}$ [44]. The Brownian motion velocity (U_{p}) is obtained from Eq. (17):

$$U_{\mathrm{p}} = \frac{2k_{\mathrm{B}}T}{\pi\mu_{\mathrm{f}}d_{\mathrm{p}}^{2}}. \tag{17}$$

Here, d_{f} and d_{p} are the diameters of water molecules and copper particles, respectively, which are 2×10^{-10} and 100×10^{-9}. It should be noted that this particular model is used for spherical nanoparticles. The volume fraction of nanoparticles should be between 1 and 8%, and the base fluid can be water and ethylene glycol.

The natural heat transfer coefficient is:

$$h_{\mathrm{nf}} = \frac{q''}{T_{\mathrm{h}} - T_{\mathrm{c}}} \tag{18}$$

The Nusselt number, whose length scale is measured based on the size of the enclosure edge, is defined as:

$$Nu = \frac{h_{\mathrm{nf}}H}{k_{\mathrm{f}}} \tag{19}$$

The heat flux of walls per unit area is:

$$q'' = -k_{\mathrm{nf}}\frac{T_{\mathrm{h}} - T_{\mathrm{c}}}{H}\left.\frac{\partial\theta}{\partial n}\right|_{\mathrm{wall}} \tag{20}$$

By placing the relations (18) and (20) into (19), the Nusselt number is obtained using relation (21):

$$Nu = -\left(\frac{k_{\mathrm{nf}}}{k_{\mathrm{f}}}\right)\left.\frac{\partial\theta}{\partial n}\right|_{\mathrm{wall}} \tag{21}$$

The average Nusselt number on the hot wall is:

$$Nu_{\mathrm{Avg}} = \frac{1}{L}\int_{0}^{1} Nu_{\mathrm{x}}\,\mathrm{d}X \tag{22}$$

Validation of the numerical scheme

In order to validate the results of the computer program, numerical simulations are performed and the results are compared with the numerical results. To verify the present results, the geometry presented by Chamkha and Abu-Nada [27] is considered for the simulations. The results are compared in Table 2. As can be seen, the relative differences between the values of the Nusselt number are negligible and, therefore, the accuracy of the present simulations is assured.

Table 2 Comparison of the average Nusselt number in mixed convection [27]

Ri	φ	Chamkha and Abu-Nada [27]	Present work	Difference percentage
0.01	0.02	32.80	33.14	1.04
	0.1	36.90	36.40	1.36
1	0.02	4.92	4.76	3.25
	0.1	4.95	4.84	2.22
10	0.02	1.72	1.68	2.32
	0.1	2.01	1.93	3.98

Grid study

In order to find an appropriate grid resolution, the average Nusselt number of water–copper nanofluid is calculated for the grid resolutions of 221 × 111, 241 × 121, 261 × 131, 281 × 141 and 301 × 151 for $\theta_s = 45$, the Reynolds number of 100, the Darcy number 10^{-2} and volume fraction of 0.02. The results are compared in Table 3. It is found that the grid resolution of 281 × 141 is appropriate. In Fig. 2, the average Nusselt number versus of number of grid for $\theta_s = 45$, $Re = 100$, $Da = 10^{-2}$ and $\varphi = 0.02$ is presented.

The convergence criterion for pressure, velocity and temperature is obtained from Eq. (23) in which M and N are the number of points in the direction of x and y, and ζ represents the variable that is solved. k is the number of iterations, and the maximum error rate is 10^{-6}.

Table 3 The average Nusselt number on the hot wall for water–copper nanofluid for $\theta_s = 45$, $Re = 100$, $Da = 10^{-2}$ and $\varphi = 0.02$

Number of grid	Grid resolution	Nu_{Avg}
1	221 × 111	3.221
2	241 × 121	3.245
3	261 × 131	3.268
4	281 × 141	3.278
5	301 × 151	3.280

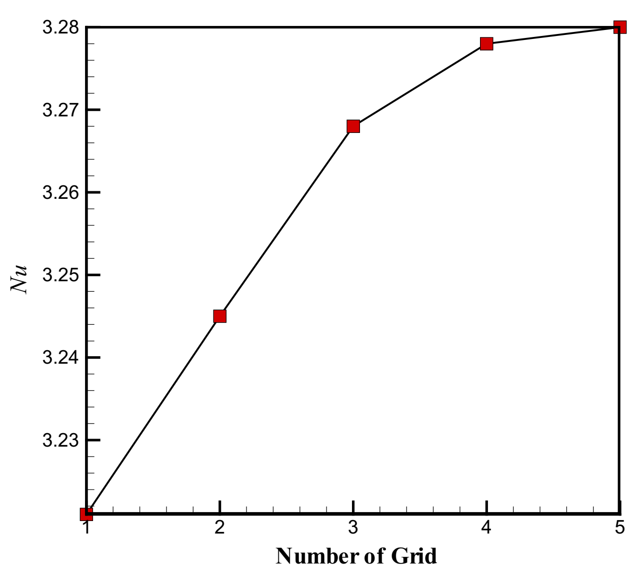

Fig. 2 The average Nusselt number versus of number of grid for $\theta_s = 45$, $Re = 100$, $Da = 10^{-2}$ and $\varphi = 0.02$

$$\text{Error} = \frac{\sum_{i=1}^{M}\sum_{j=1}^{N}\left|\zeta_{i,j}^{k+1} - \zeta_{i,j}^{k}\right|}{\sum_{i=1}^{M}\sum_{j=1}^{N}\left|\zeta_{i,j}^{k+1}\right|} \leq 10^{-6} \tag{23}$$

Results

Variation in vertical velocity component

In Fig. 3, the variations in vertical velocity component for the central height versus x are shown for various Darcy numbers at $Re = 2000$ and $\varphi = 0.02$. This quantity can be a measure of the convection and movement of the nanofluid. The variation in vertical velocity component is higher at $Da = 10^{-2}$ for all leg angles, and the largest amount is related to the right region of the cavity.

The maximum and minimum velocity changes increase by increasing the leg angle of the trapezoidal enclosure. For example, maximum velocity is 0.31 and 0.325 for the leg angles of 30° and 60°, respectively, representing an increase of 5%. By reducing the Darcy number or reducing the porosity of the medium, the changes of the velocity become much more smooth compared to $Da = 10^{-2}$, as the values of the vertical component of the velocity approach zero. These variations in velocity indicate a change in the behavior of the nanofluid from mixed convection to natural one and conduction by decreasing the Darcy number.

Evaluation of streamlines and isotherms

In Fig. 4, streamlines and isothermal lines are shown for copper–water nanofluid for different Darcy and Reynolds numbers at $\varphi = 0.02$. Considering this figure, the streamlines appear as two vortices for all Reynolds numbers. The large initial vortex is affected by the lid-driven. This initial vortex has an enough velocity to move the fluid in the right-hand corner of the cavity. Hence, the secondary vortex is generated due to the effect of this velocity. As the Reynolds number increases, which actually indicates that the lid-driven is higher, the center of the first vortex moves to the right-hand side of the enclosure and causes smaller and stronger secondary vortex to form in the corner of the cavity.

As mentioned above, this behavior is observed at all Reynolds numbers. The curvature of the streamlines in the initial vortex decreases, and the secondary vortex becomes smaller by decreasing the Darcy number. The reason is a reduction in the convection and motion of nanofluid by decreasing the Darcy number. At the Darcy number of 10^{-4}, streamlines become parallel to each other, indicating a change in the behavior of the nanofluid from mixed

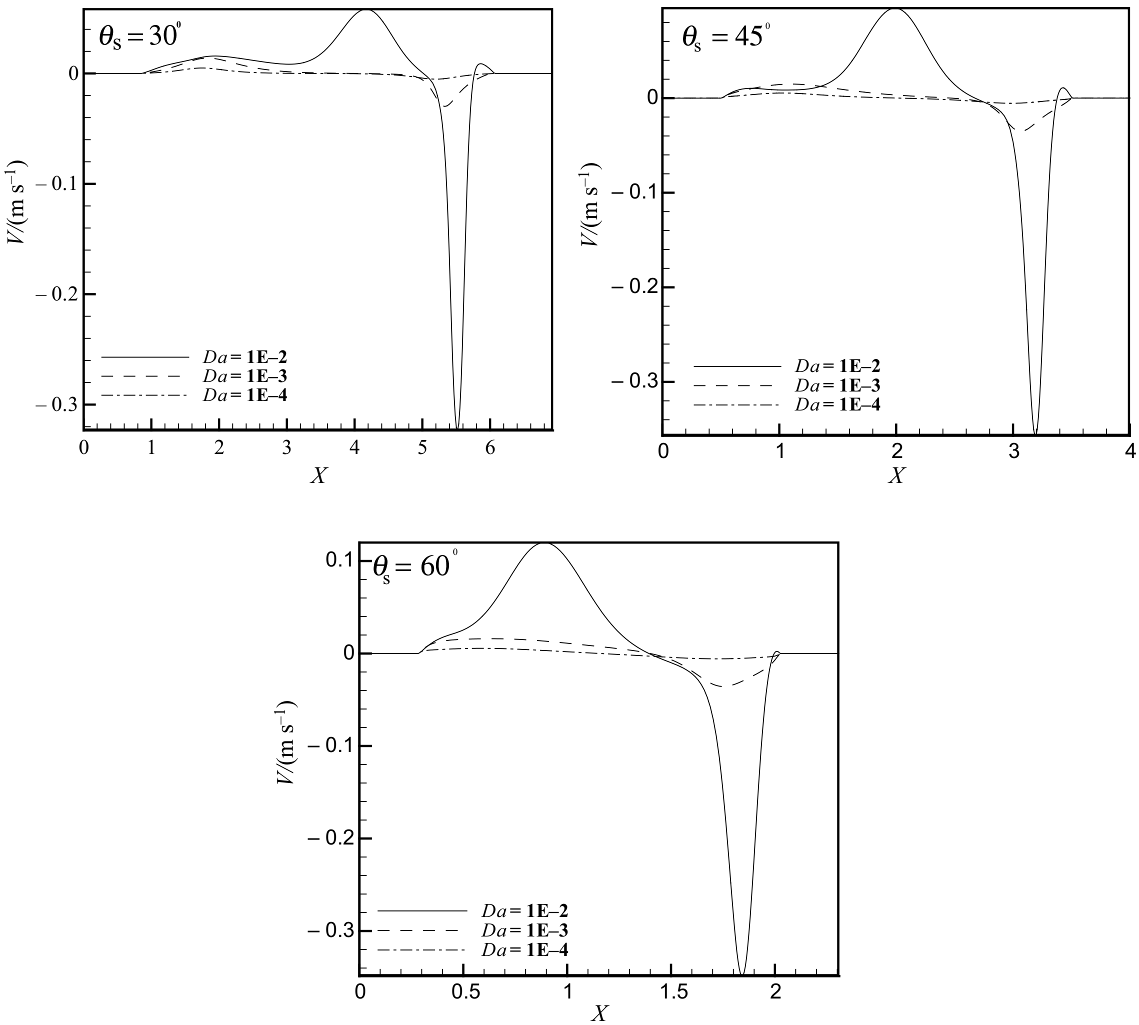

Fig. 3 The variation in vertical velocity component at mid-height versus x for different Darcy numbers at Re = 2000 and φ = 0.02

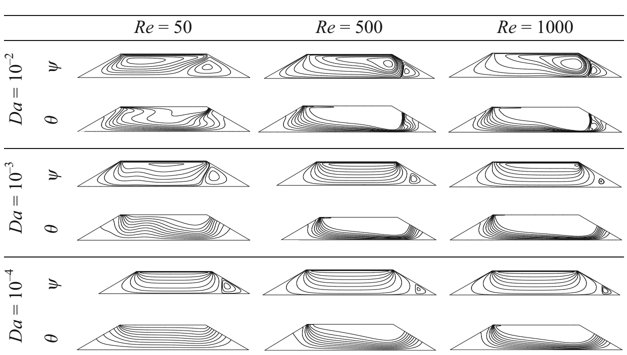

Fig. 4 Streamlines and isothermal lines for copper–water nanofluid for different Darcy and Reynolds numbers at φ = 0.02

convection to natural convection and conduction. At the Darcy number of 10^{-2}, isothermal lines have more curvature than other Darcy numbers. The curvature indicates that the porosity of the medium is such that the nanofluid can maintain its movement and convection. At this Darcy number, the density of the isothermal lines in the lower part of the trapezoid enclosure increases, especially in the right corner, by increasing the Reynolds number. The density of isothermal lines is greater in the vicinity of large and small vortices. Higher density of isothermal lines represents a higher temperature gradient and hence the higher the heat transfer in these regions. Since this behavior is proportional to the increase of the Reynolds number and hence the increase in the nanofluid convection, this behavior is reasonable. The curvature of isothermal lines decreases by decreasing the Darcy number (decreasing the porosity of the media) for constant Reynolds numbers. This behavior is due to the dominance of conduction. However, the density of isothermal lines increases with increasing Reynolds number in the lower part of the enclosure for small Darcy numbers. In Figs. 5 and 6, the streamlines and isothermal lines for the copper–water nanofluid for different Darcy and Reynolds numbers at φ = 0.02 and leg angles of 45° and 60° are presented.

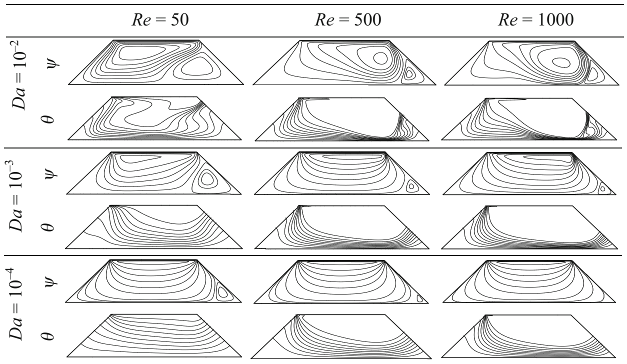

Fig. 5 Streamlines and isotherms of water–copper nanofluid at φ = 0.02 for different Reynolds and Darcy numbers and θ_s = 45°

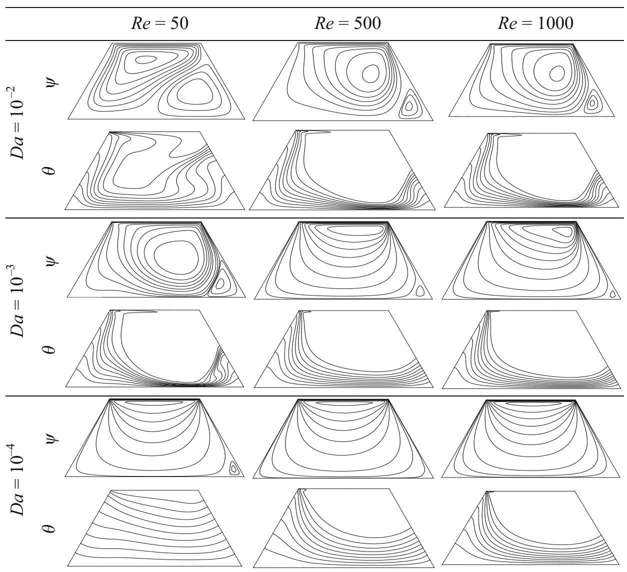

Fig. 6 Streamlines and isotherms of water–copper nanofluid at φ = 0.02 for different Reynolds and Darcy numbers and θ_s = 60°

At leg angles of 45° and 60°, the behavior of streamlines and isotherms is similar to the angle of 30°. At constant Reynolds numbers, the curvature of the streamlines is reduced and they tend to be parallel to each other with decreasing the Darcy number, which is equivalent to decreasing of the porosity of the media. This behavior shows the decrease in nanofluid movement in the enclosure. Also, in these two angles, the center of the initial vortex is shifted to the right side of the enclosure and the second vortex becomes smaller by increasing the Reynolds number at a constant Darcy number. At 45° and 60°, the density of isothermal lines increases close to the bottom of the hot wall and on the right side of the enclosure for different Reynolds and Darcy numbers.

Variation in the Nusselt number

In Figs. 7–9, the variations in the average Nusselt number as a function of the volume fraction of nanoparticles are shown at the leg angles of 30°, 45° and 60° for different Darcy and Reynolds numbers. The average Nusselt number increases by increasing the volume fraction of the nanoparticles for different leg angles and Darcy numbers. In fact, the thermal conductivity of the nanofluid and the heat transfer increase with increasing volume fraction of nanoparticles. At a constant leg angle, the average Nusselt number decreases with the reduction in the Darcy number (reduction in the convection and the motion of the nanofluid). The variations in the average Nusselt number are close to each other in terms of volume fraction at Reynolds numbers of 10, 50 and 100, but the variation in average Nusselt number increases by increasing the Reynolds number to 500 and 1000, which leads to the overcoming of forced convection on natural one.

At θ_s = 30° and $Da = 10^{-2}$, the average Nusselt number increases by 1.78 times with the increase in Reynolds number from 10 to 1000. This increase is the same for different volume fractions. For $Da = 10^{-3}$, the average Nusselt number increases by 3.53 times with the increase in Reynolds number from 10 to 1000 for the volume fraction of 0.02. Also, for $Da = 10^{-4}$, the average Nusselt number increases by 2.23 times with the increase in Reynolds number from 10 to 1000 for the volume fraction of 0.0.

At leg angles of 45° and 60°, the behavior of the average Nusselt number is similar to that for the leg angle of 30° by increasing the volume fraction of the nanoparticles and different Darcy and Reynolds numbers.

At θ_s = 45° and Da = 10^{-2}, the average Nusselt number increases by 2.23 times with the increase in Reynolds number from 10 to 1000 for the volume fraction of 0.01. At Da = 10^{-3}, the average Nusselt number increases by 4.08 times with the increase in Reynolds number from 10 to 1000 for the volume fraction of 0.01. Also, for Da = 10^{-4}, the average Nusselt number increases by 2.66 times with the increase in Reynolds number from 10 to 1000 for the volume fraction of 0.0.

At θ_s = 60° and Da = 10^{-2}, the average Nusselt number increases by 2.28 times with the increase in Reynolds number from 10 to 1000 for the volume fraction of 0.04. For Da = 10^{-3}, the average Nusselt number increases by 3.95 times with the increase in Reynolds number from 10 to 1000 for the volume fraction of 0.01. Also, for Da = 10^{-4} the average Nusselt number increases by 2.34 times with the increase in Reynolds number from 10 to 1000 for the volume fraction of 0.0.

The average Nusselt number increases by increasing the leg angle of the trapezoid for all Reynolds numbers.

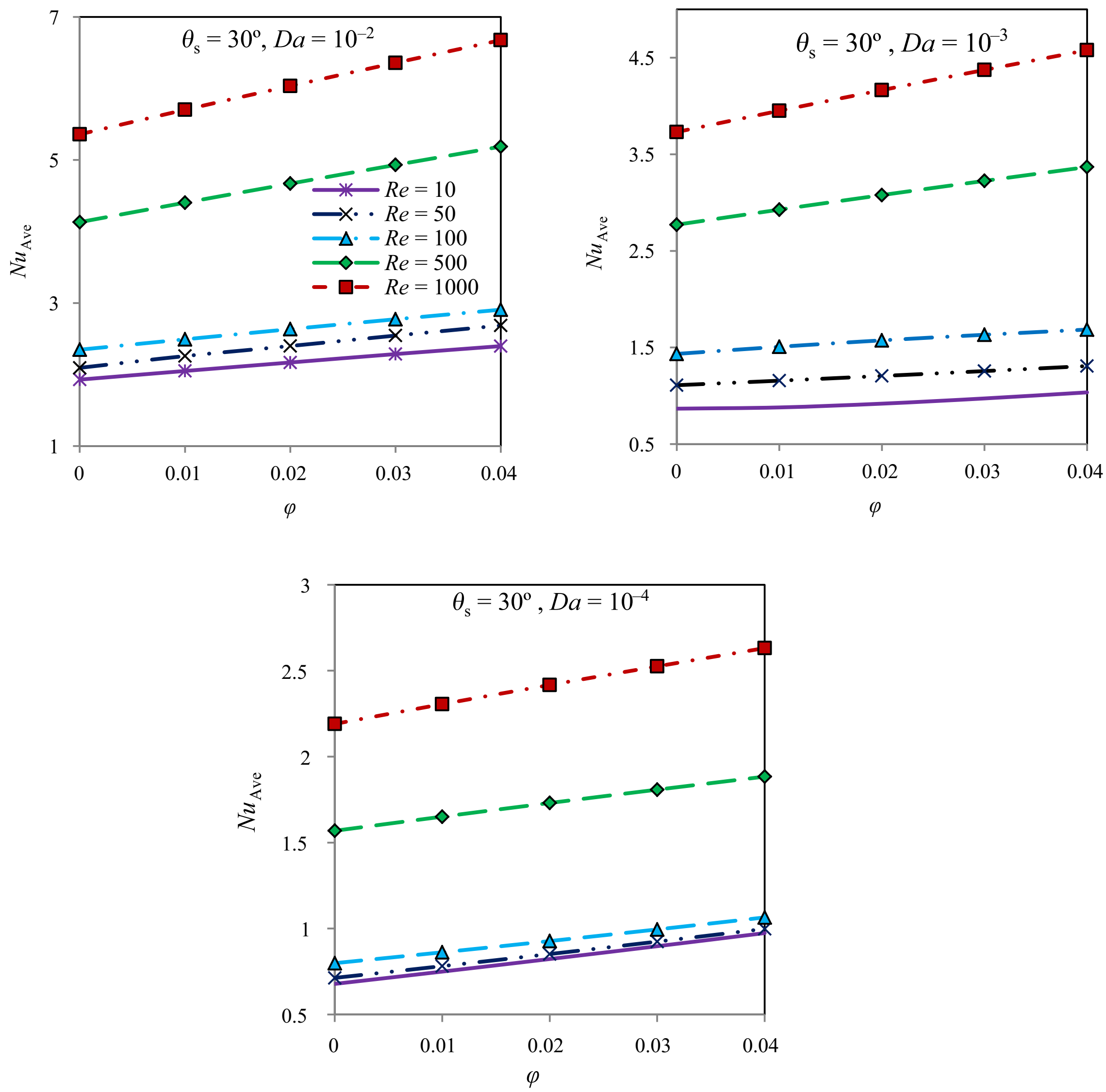

Fig. 7 The average Nusselt number versus the volume fraction of nanoparticles at $\theta_s = 30°$ for various Darcy numbers

However, the enclosure becomes smaller and the motion and convection of the nanofluid are further limited with the increase in the leg angle of the cavity. In fact, with an increase in the leg angle, though the nanofluid has less space to move, the temperature gradient increases in the enclosure. In other words, the local Nusselt number increases and therefore the average Nusselt number increases. For example, for $Da = 10^{-2}$ at leg angles of 30°, 45° and 60° at Reynolds number of 1000 and zero volume fraction, the average Nusselt number is 5.36, 6.71 and 8.50 and at the volume fraction of 0.04% is equal to 6.86, 8.40 and 10.90, respectively. These results show the increase in the Nusselt number and its variation with the volume fraction by increasing the leg angle.

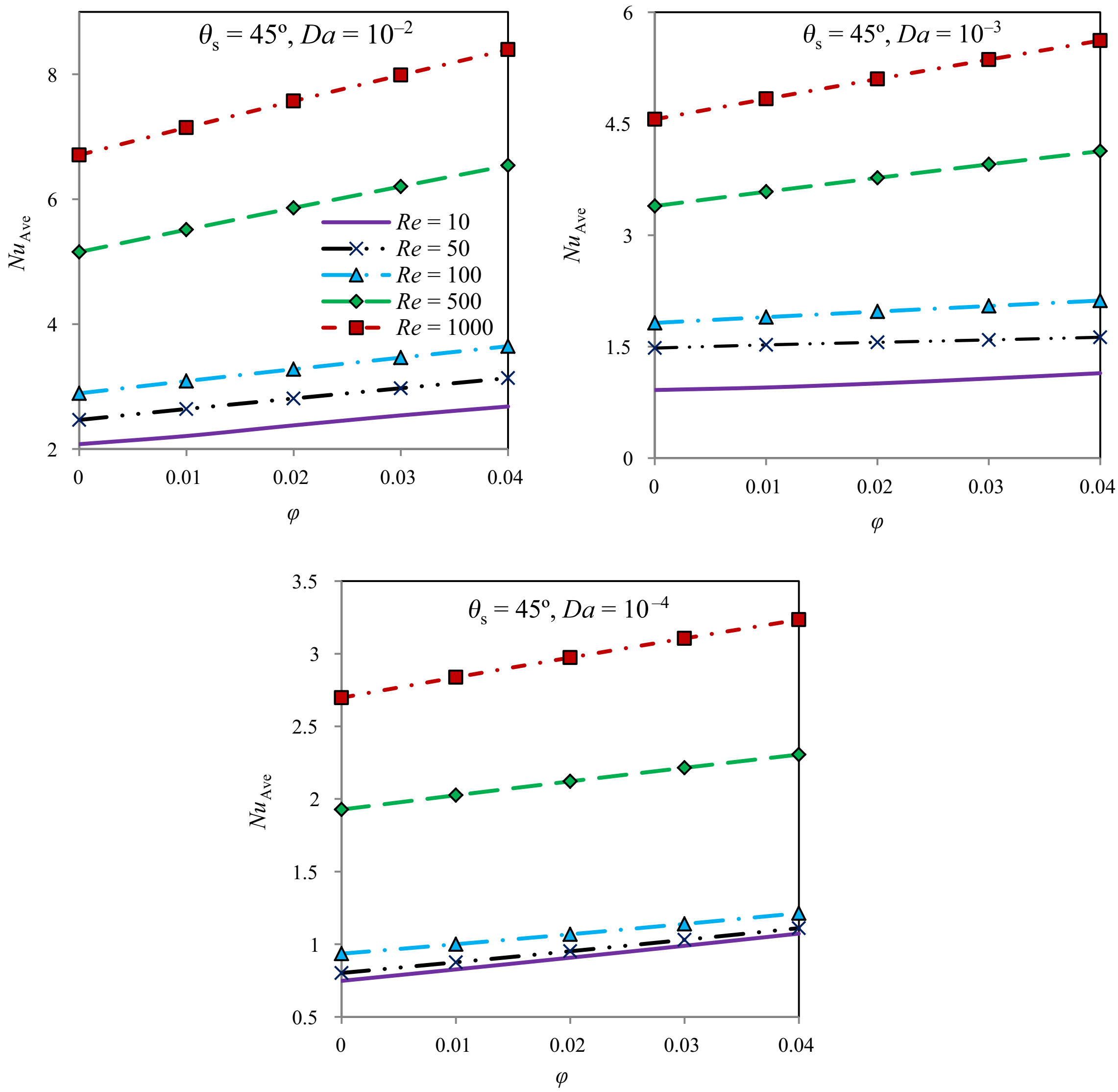

Fig. 8 The average Nusselt number versus the volume fraction of nanoparticles at θ_s = 45° for various Darcy numbers

Variation in the average Nusselt number with the Reynolds number

In order to evaluate the changes in the Nusselt number, the average Nusselt number is shown in Fig. 10 as a function of the Reynolds number for different Darcy numbers, volume fractions and leg angles.

For all cases examined, the average Nusselt number increases with the Reynolds number due to the increase in nanofluid convection. At Reynolds number of 10 for Darcy numbers of 10^{-3} and 10^{-4}, the average Nusselt number is almost the same. This indicates that the porosity of the media has little effect at low Reynolds numbers unless the porosity increases.

The difference in the average Nusselt number increases with the Reynolds number for different volume fractions, leg angles and Darcy numbers. The highest difference is observed at the Reynolds number of 1000. Also, this

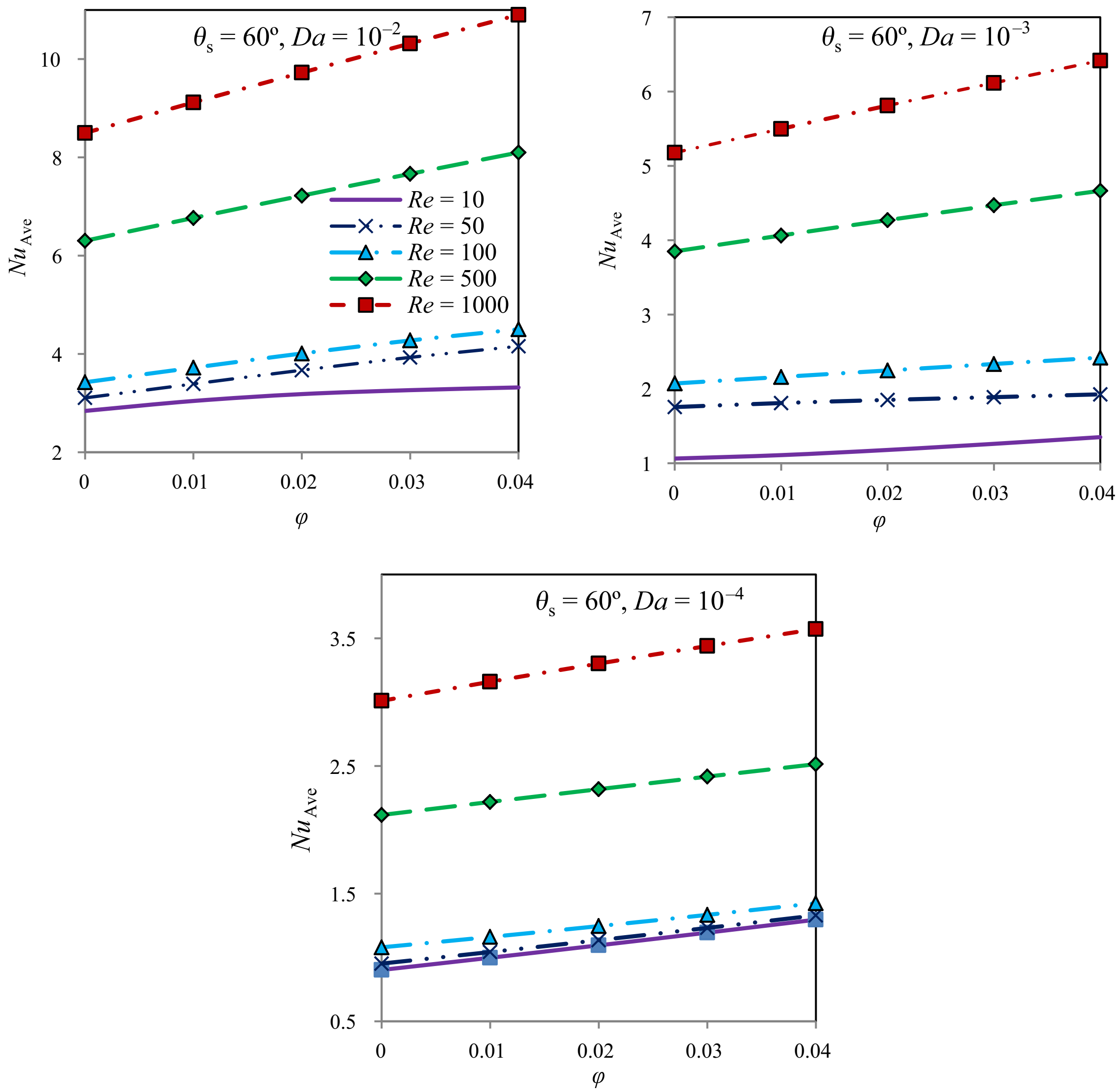

Fig. 9 The average Nusselt number versus the volume fraction of nanoparticles at θ_s = 60° for various Darcy numbers

difference in the Nusselt number is more considerable at larger leg angles.

Variation in local Nusselt number

In Fig. 11, the variation in the local Nusselt number on the lower hot wall is shown in terms of x for various Darcy numbers at Re = 1000 and φ = 0.02. The maximum amount of local Nusselt number is almost identical at different leg angles. By increasing the leg angle, the maximum range of local Nusselt number increases. This increase in the maximum range of local Nusselt number by increasing the leg angle leads to an increase in the average Nusselt number. By decreasing the Darcy number, the variation curve of the local Nusselt number becomes smoother and its values drop sharply. As previously mentioned, the cause of this behavior is due to the limitation in

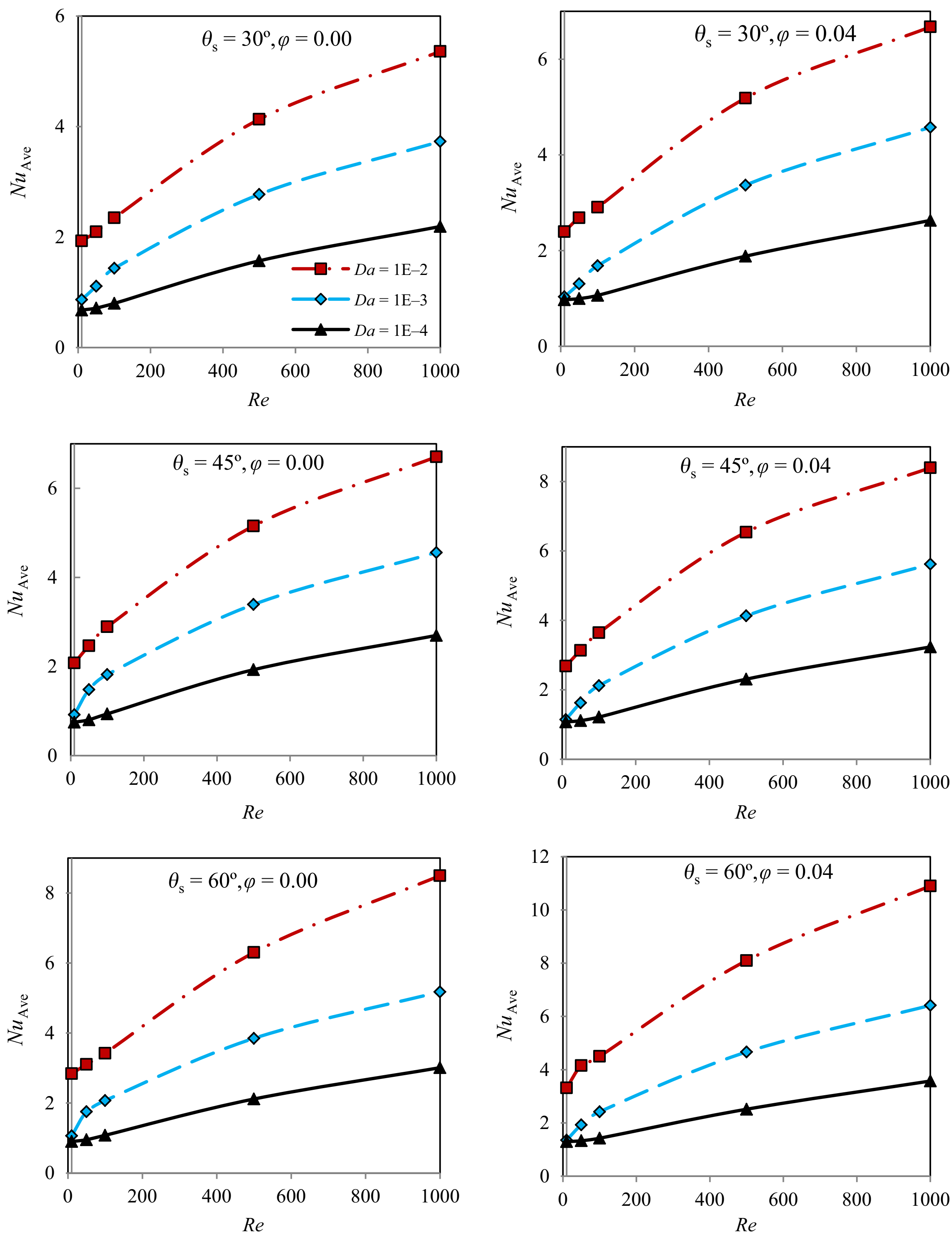

Fig. 10 The average Nusselt number versus the Reynolds number for different volume fractions and leg angles

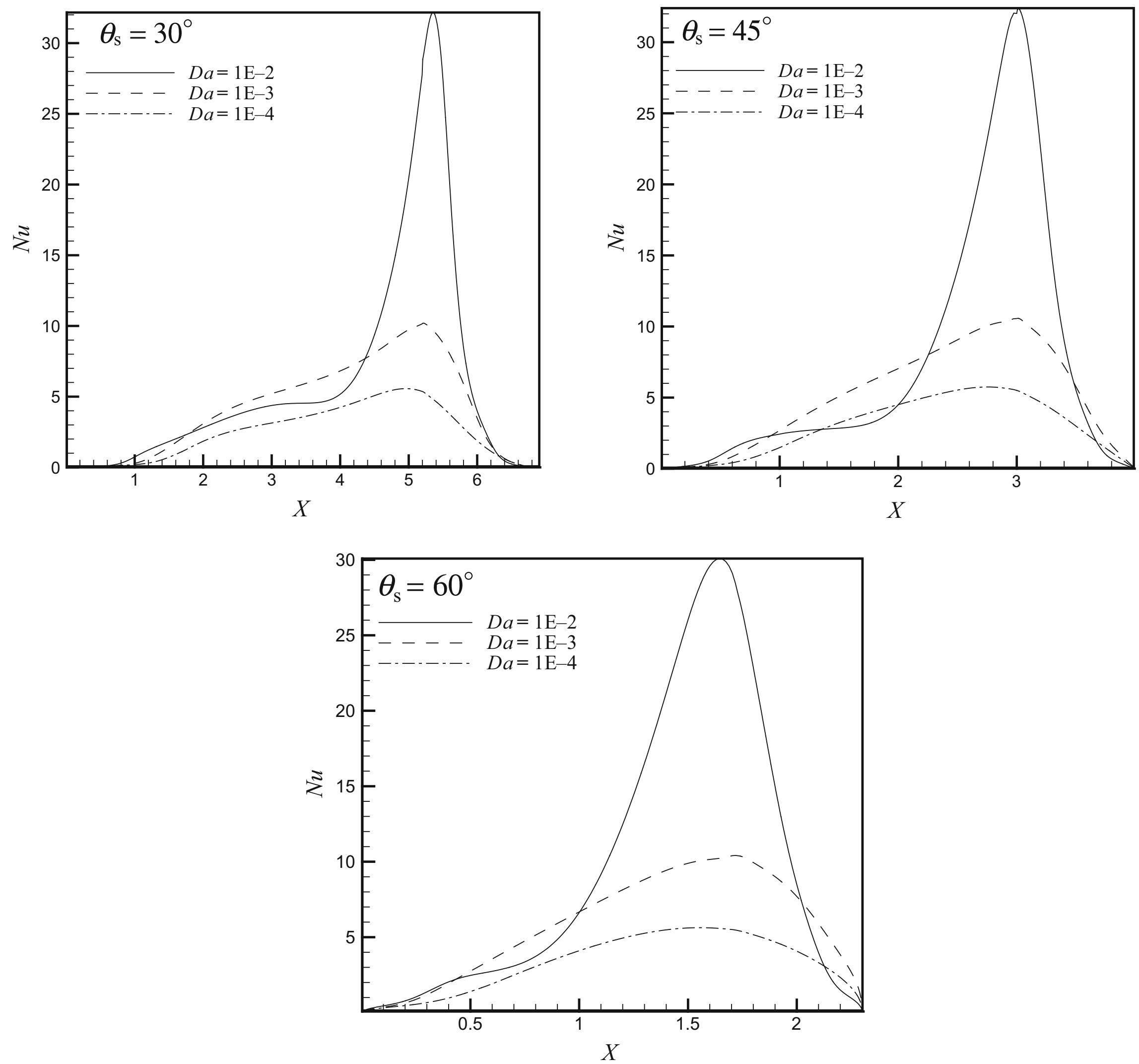

Fig. 11 Local Nusselt number on a lower hot wall in terms of x for various Darcy numbers at Re = 1000 and φ = 0.02

the convection and motion of the nanofluid with the reduction in the Darcy number.

Conclusions

In the present study, the flow field and heat transfer of a water–copper nanofluid with variable properties in a trapezoidal enclosure saturated with porous media are studied. The study is conducted for aspect ratios of 30°, 45° and 60°, Reynolds numbers from 10 to 1000, Darcy numbers of 10^{-2}, 10^{-3}, 10^{-4} and volume fractions of 0 to 0.04 of nanoparticles. The following results were obtained:

1. Numerical results show that the average Nusselt number increases with increasing volume fraction of nanoparticles for all studied Darcy numbers.
2. The convection and motion of the nanofluid decrease by reducing the Darcy number which leads to a reduction in the velocity and local Nusselt number.
3. The average Nusselt number increases by increasing the Darcy number for all aspect ratios.
4. The average Nusselt number increases with increasing Reynolds number for all Darcy numbers, aspect ratios and volume fractions of nanoparticles.
5. At leg angles of 45° and 60°, the behavior of streamlines and isotherms is similar to the angle of 30°.
6. The average Nusselt number increases by increasing the leg angle of the trapezoid for all Reynolds numbers.

References

1. Nojoomizadeh M, D'Orazio A, Karimipour A, Afrand M, Goodarzi M. Investigation of permeability effect on slip velocity and temperature jump boundary conditions for FMWNT/Water nanofluid flow and heat transfer inside a microchannel filled by a porous media. Phys E. 2018;97:226–38.
2. Nojoomizadeh M, Karimipour A, Firouzi M, Afrand M. Investigation of permeability and porosity effects on the slip velocity and convection heat transfer rate of Fe_3O_4/water nanofluid flow in a microchannel while its lower half filled by a porous medium. Int J Heat Mass Transf. 2018;119:891–906.
3. Meghdadi Isfahani AH, Tasdighi I, Karimipour A, Shirani E, Afrand M. A joint lattice Boltzmann and molecular dynamics investigation for thermohydraulical simulation of nano flows through porous media. Eur J Mech B Fluids. 2016;55:15–23.
4. Meghdadi Isfahani AH, Afrand M. Experiment and Lattice Boltzmann numerical study on nanofluids flow in a micromodel as porous medium. Phys E. 2017;94:15–21.
5. Afrand M, Esfe MH, Abedini E, Teimouri H. Predicting the effects of magnesium oxide nanoparticles and temperature on the thermal conductivity of water using artificial neural network and experimental data. Phys E. 2017;87:242–7.
6. Afrand M, Karimipour A, Nadooshan AA, Akbari M. The variations of heat transfer and slip velocity of FMWNT-water nanofluid along the micro-channel in the lack and presence of a magnetic field. Phys E. 2016;84:474–81.
7. Akbari M, Afrand M, Arshi A, Karimipour A. An experimental study on rheological behavior of ethylene glycol based nanofluid: proposing a new correlation as a function of silica concentration and temperature. J Mol Liq. 2017;233:352–7.
8. Asadi A, Asadi M, Rezaniakolaei A, Rosendahl LA, Afrand M, Wongwises S. Heat transfer efficiency of Al_2O_3-MWCNT/thermal oil hybrid nanofluid as a cooling fluid in thermal and energy management applications: an experimental and theoretical investigation. Int J Heat Mass Transf. 2018;117:474–86.
9. Dehkordi RA, Esfe MH, Afrand M. Effects of functionalized single walled carbon nanotubes on thermal performance of antifreeze: an experimental study on thermal conductivity. Appl Therm Eng. 2017;120:358–66.
10. Esfahani NN, Toghraie D, Afrand M. A new correlation for predicting the thermal conductivity of ZnO–Ag (50%–50%)/water hybrid nanofluid: an experimental study. Powder Technol. 2018;323:367–73.
11. Esfe MH, Bahiraei M, Hajmohammad MH, Afrand M. Rheological characteristics of MgO/oil nanolubricants: experimental study and neural network modeling. Int Commun Heat Mass Transf. 2017;86:245–52.
12. Esfe MH, Motahari K, Sanatizadeh E, Afrand M, Rostamian H, Ahangar MRH. Estimation of thermal conductivity of CNTs-water in low temperature by artificial neural network and correlation. Int Commun Heat Mass Transf. 2016;76:376–81.
13. Nadooshan AA, Esfe MH, Afrand M. Evaluation of rheological behavior of 10W40 lubricant containing hybrid nano-material by measuring dynamic viscosity. Phys E. 2017;92:47–54.
14. Nadooshan AA, Esfe MH, Afrand M. Prediction of rheological behavior of SiO_2-MWCNTs/10W40 hybrid nanolubricant by designing neural network. J Therm Anal Calorim. 2018;131:2741–8.
15. Nadooshan AA, Eshgarf H, Afrand M. Measuring the viscosity of Fe_3O_4-MWCNTs/EG hybrid nanofluid for evaluation of thermal efficiency: newtonian and non-Newtonian behavior. J Mol Liq. 2018;253:169–77.
16. Ranjbarzadeh R, Karimipour A, Afrand M, Isfahani AHM, Shirneshan A. Empirical analysis of heat transfer and friction factor of water/graphene oxide nanofluid flow in turbulent regime through an isothermal pipe. Appl Therm Eng. 2017;126:538–47.
17. Sepyani K, Afrand M, Esfe MH. An experimental evaluation of the effect of ZnO nanoparticles on the rheological behavior of engine oil. J Mol Liq. 2017;236:198–204.
18. Shahsavani E, Afrand M, Kalbasi R. Experimental study on rheological behavior of water–ethylene glycol mixture in the presence of functionalized multi-walled carbon nanotubes. J Therm Anal Calorim. 2018;131:1177–85.
19. Shahsavani E, Afrand M, Kalbasi R. Using experimental data to estimate the heat transfer and pressure drop of non-Newtonian nanofluid flow through a circular tube: applicable for use in heat exchangers. Appl Therm Eng. 2018;129:1573–81.
20. Mahian O, Kolsi L, Amani M, Estellé P, Ahmadi G, Kleinstreuer C, Marshall JS, Siavashi M, Taylor RA, Niazmand H, Wongwises S, Hayat T, Kolanjiyil A, Kasaeian A, Pop I. Recent advances in modeling and simulation of nanofluid flows—part I: fundamentals and theory. Phys Rep. 2019;790:1–48.
21. Mahian O, Kolsi L, Amani M, Estellé P, Ahmadi G, Kleinstreuer C, Marshall JS, Taylor RA, Abu-Nada E, Rashidi S, Niazmand H, Wongwises S, Hayat T, Kasaeian A, Pop I. Recent advances in modeling and simulation of nanofluid flows—part II: applications. Phys Rep. 2019;791:1–59.
22. Noori Rahim Abadi SMA, Jafari A. Investigating the natural convection heat transfer from two elliptic cylinders in a closed cavity at different cylinder spacings. Heat Transf Res. 2012;43(3):259–84.
23. Mansour MA, Mohamed RA, Abd-Elaziz MM, Ahmed SE. Numerical simulation of mixed convection flows in a square lid-driven cavity partially heated from below using nanofluid. Int Commun Heat Mass Transf. 2010;37:1504–12.
24. Ghasemi B, Aminossadati SM. Mixed convection in a lid-driven triangular enclosure filled with nanofluids. Int Commun Heat Mass Transf. 2010;37:1142–8.
25. Sheikhzadeh GA, Ebrahim Qomi M, Hajialigol N, Fattahi A. Numerical study of mixed convection flows in a lid-driven enclosure filled With nanofluid using variable properties. Int Res Phys. 2012;2:5–13.
26. Pishkar I, Ghasemi B. Cooling enhancement of two fins in a horizontal channel by nanofluid mixed convection. Int J Therm Sci. 2012;59:141–51.
27. Chamkha AJ, Abu-Nada E. Mixed convection flow in single- and double-lid driven square cavities filled with water–Al_2O_3 nanofluid: effect of viscosity models. Eur J Mech B/Fluids. 2012;36:82–96.
28. Abbasian Arani AA, MazroueiSebdani S, Mahmoodi B, Ardeshiri M, Aliakbari A. Numerical study of mixed convection flow in a lid-driven cavity with sinusoidal heating on sidewalls using nanofluid. Superlattices Microstruct. 2012;51:893–911.
29. Oztop HF, Al-Salem K, Varol Y, Pop I. Natural convection heat transfer in a partially opened cavity filled with porous media. Int J Heat Mass Transf. 2011;54:2253–61.
30. Bourantas GC, Skouras ED, Loukopoulos VC, Burganos VN. Heat transfer and natural convection of nanofluids in porous media. Eur J Mech B/Fluid. 2014;43:45–56.
31. Hajipour M, Molaei A. DehkordiMixed-convection flow of Al_2O_3–H_2O nanofluid in a channel partially filled with porous metal foam: experimental and numerical study. Exp Thermal Fluid Sci. 2014;51(53):49–56.
32. Nielda DA, Kuznetsov AV. Forced convection in a parallel-plate channel occupied by a nanofluid or a porous medium saturated by a nanofluid. Int J Heat Mass Transf. 2014;70:430–3.
33. Abedini E, Zarei T, Rajabnia H, Kalbasi R, Afrand M. Numerical investigation of vapor volume fraction in subcooled flow boiling of a nanofluid. J Mol Liq. 2017;238:281–9.

34. Afrand M. Using a magnetic field to reduce natural convection in a vertical cylindrical annulus. Int J Therm Sci. 2017;118:12–23.
35. Afrand M, Farahat S, Nezhad AH, Ali Sheikhzadeh G, Sarhaddi F. 3-D numerical investigation of natural convection in a tilted cylindrical annulus containing molten potassium and controlling it using various magnetic fields. Int J Appl Electromagn Mech. 2014;46:809–21.
36. Afrand M, Farahat S, Nezhad AH, Sheikhzadeh GA, Sarhaddi F. Numerical simulation of electrically conducting fluid flow and free convective heat transfer in an annulus on applying a magnetic field. Heat Transf Res 2014;45:749–66.
37. Afrand M, Farahat S, Nezhad AH, Sheikhzadeh GA, Sarhaddi F, Wongwises S. Multi-objective optimization of natural convection in a cylindrical annulus mold under magnetic field using particle swarm algorithm. Int Commun Heat Mass Transf. 2015;60:13–20.
38. Afrand M, Rostami S, Akbari M, Wongwises S, Esfe MH, Karimipour A. Effect of induced electric field on magneto-natural convection in a vertical cylindrical annulus filled with liquid potassium. Int J Heat Mass Transf. 2015;90:418–26.
39. Pordanjani AH, Nadooshan AA, Afrand M. Effect of two isothermal obstacles on the natural convection of nanofluid in the presence of magnetic field inside an enclosure with sinusoidal wall temperature distribution. Int J Heat Mass Transf. 2018;121:565–78.
40. Ali Karimi MA. Numerical study on thermal performance of an air-cooled heat exchanger: effects of hybrid nanofluid, pipe arrangement and cross section. Energy Convers Manag. 2018;164:615–28.
41. Teimouri H, Afrand M, Sina N, Karimipour A, Isfahani AHM. Natural convection of liquid metal in a horizontal cylindrical annulus under radial magnetic field. Int J Appl Electromagn Mech. 2015;49:453–61.
42. Abu-Nada E, Masoud Z, Hijazi A. Natural convection heat transfer enhancement in horizontal concentric annuli using nanofluids. Int Commun Heat Mass Transf. 2008;35:657–65.
43. Brinkman HC. The viscosity of concentrated suspensions and solution. J Chem Phys. 1952;20:571–81.
44. Patel HE, Sundararajan T, Pradeep T, Dasgupta A, Dasgupta N, Das SK. A micro-convection model for thermal conductivity of nanofluids. J Phys. 2005;65:863–9.